A Review on Electrical Submersible Pump Head Losses and Methods to Analyze Two-Phase Performance Curve

SALMAN SHAHID
Department of Mechanical Engineering
Abu Dhabi University
Abu Dhabi, P.O. Box 59911
UNITED ARAB EMIRATES

SHARUL SHAM DOL*
Department of Mechanical Engineering
Abu Dhabi University
Abu Dhabi, P.O. Box 59911
UNITED ARAB EMIRATES

ABDUL QADER HASAN
Department of Mechanical Engineering
Abu Dhabi University
Abu Dhabi, P.O. Box 59911
UNITED ARAB EMIRATES

OMAR MUSTAFA KASSEM
Department of Mechanical Engineering
Abu Dhabi University
Abu Dhabi, P.O. Box 59911
UNITED ARAB EMIRATES

MOHAMED S. GADALA
Department of Mechanical Engineering
Abu Dhabi University
Abu Dhabi, P.O. Box 59911
UNITED ARAB EMIRATES

MOHD SHIRAZ ARIS
TNB Research Sdn. Bhd.
Kawasan Institusi Penyelidikan
43000 Kajang
Selangor Darul Ehsan
MALAYSIA

Abstract: - Electrical submersible pumps (ESP) are referred to as a pump classification whose applications are based upon transporting fluids from submersible elevations towards a fixed pipeline. Specific ESP pumps are utilized in offshore oil and gas facilities that are frequently employed in transport of Liquefied Natural Gas (LNG) terminals. Transport of LNG is a multiphase process that causes operational challenges for ESP due to presence of air pockets and air bubbles; presenting difficulties, such as cavitation and degradation to pump components. This performance degradation causes an economic risk to companies as well as a risk to pump performance capabilities, as it will not be able to pump with the same pressure again. Operational references for multiphase flow in ESP are limited; thus, this research paper reports multistage pumping, review of fundamentals, previous experimental as well as modelling work benefitting future literature for a potential solution. Industries consume power to cope up with the losses associated with pumping two-phase fluids causing company's fortune. Preceding experimental work on single along with multiphase flow illustrate a distinct flow pattern surrounding the area around pump impeller while the pump is in operation. Through experimental observation, four flow patterns were observed and studied when gas was varied at different flow rates. Increasing the intake pressure proved to increase pump performance at two-phase flow. Experimental study of multiphase flow with LNG fluid is expensive; thus, experimental validation is accomplished on a single stage pump with external intervention of air bubbles to simulate LNG vaporization at fixed pressure and temperature difference.

Key-Words: - Electrical Submersible Pump; Head loss; LNG; Multiphase; Performance curve; CFD; Turbulence

Nomenclature

Q	Flow rate	ρ	Density
C_d	Gravitational acceleration	τ_{shock}	Shock coefficient
H	Pump Head	Q_{lk}	Volume of leaked fluid
h_P	Head Pressure	U_{lk}	Velocity of leaked fluid
P_d	Absolute outlet pressure	ξ	Inlet loss coefficient
P_S	Absolute inlet pressure	ξ_e	Exit loss
V_w	Projection of absolute velocities	L	Seal length
U	Peripheral velocity	C	Seal clearance
f	Friction coefficient	D_f	Diffuser factor

D_H	Hydraulic Head	K	Coefficient of loss
R	Radius	f_{TD}	Local drag coefficient
D	Diameter	E_c	Empirical constant
Re	Reynolds Number	h	Channel height
W	Relative fluid velocity	K_{RR}	Friction factor
H_r	Hydraulic radius	Ψ	Head coefficient
$C_{r,wake}$	Radial velocity of the wake	α	Flow angle
$C_{r,mix}$	Radial velocity of mixed flow	β	Blade angle
ΔP_{cl}	Pressure difference across the gap	ε	Surface roughness
$\dot{m}_{cl}$	Clearance gap leakage flow rate	λ	Friction resistance coefficient
ω_{cl}	Clearance loss	ω	Rotational Speed

1 Introduction

Centrifugal pumps are commonly put to use in a number of areas ranging from domestic utilization to extensive industrial applications. These pumps are premeditated to use water or other incompressible fluids with a limitation on viscosity; however, some industrial processes require liquid-gas mixture as their working fluid, such as pressurized water reactors, and these pumps are not designed to handle two-phase flow. The electrical submersible pump (ESP) system is a derivative of the centrifugal pump where the fluid source is characteristically located underneath the discharge datum. These systems are utilized in the petroleum industry to improve the production of wells that contain gas as a residual product creating an oil and gas mixture [1].

ESPs are actually the most extensively utilized artificial lift method in the oil and gas industry for maintaining a high crude-oil production [2]. An ESP contains some key components used especially for offshore oil production wells, such as an impeller and a diffuser per stage. The impeller rotates according to the shaft, that increases the kinetic energy of the initial flow and depends on the diffuser to convert that kinetic energy into potential energy for the next stage. These components need to be assembled in a series of stages as shown in Fig. 1. The gases formed from this process contributes negatively to the pump resulting in loss of pump performance causing safety issues, economic losses and other effects [1]. Higher gas presence causes gas pocket formation at the impeller blades locking the flow channel and resisting fluid flow [2].

Earlier studies emphasized that occurrence of gas in Electrical Submersible Pump causes hydraulic head degradation, and that flow behavior under gassy conditions and pressure surging deteriorates the head further. Although ESPs are getting used to gas-liquid mixture flow, the exact mechanism behind the head deterioration due to two-phase flow is still unclear. Variables, such as bubble coalescence and breakup mechanisms are quite difficult to visualize due to the complex geometry of multistage ESP [3]. Some relevant studies can be found in [4] and [5].

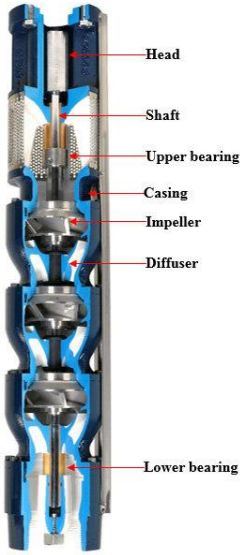

Figure 1: Major components in a multi-stage Electrical Submersible Pump [3]

This paper provides a comprehensive review on various ESP pump head losses that have been investigated in previous literature using both experimental and simulation techniques to examine two-phase flow. A number of studies are focused upon centrifugal pump performance under two phase conditions that are accessible in literature; however, further research is required on multiphase flow mechanisms inside a rotating impeller of an ESP [2]. Finally, this paper provides useful guidance on closing gaps for upcoming researches and to assess researchers contributing in multistage and multiphase pumping systems.

1.1 Performance Curve

A typical pump performance curve indicates pumps operation under a certain pressure head and flow rate. These curves are described in terms of particular pump operating speed (rpm) and inlet/outlet diameter. The curve has the pumps flow rate directed towards the x-axis while pressure head is designated on the y-axis as shown in Fig. 2, which shows a single stage pump performance curve at 50 Hz speed and 20°C working fluid. Some curves also provide the user with the Best Efficiency Point (BEP) that proportionate to the maximum efficiency range. At the BEP, the pump's impeller is exposed to minimum amount of radial force providing smooth operation with low vibration and noise. A pump performance curve unites the pressure head and flow range which is characteristically used by designers and operatives to evaluate the functioning region of the pump.

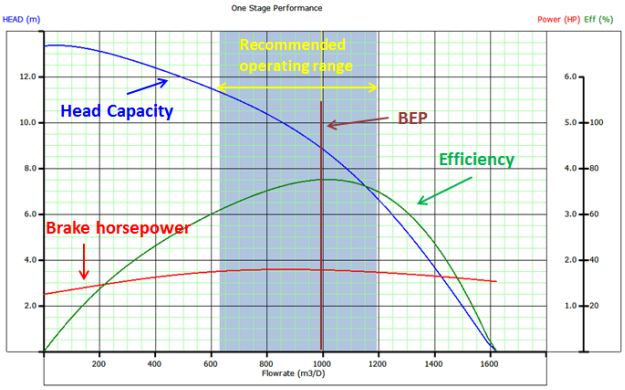

Figure 2: Typical Pump Performance Curve [6]

Visualization of flow patterns inside an ESP with a flow of gas/liquid mixture requires tough investigation using a transparent casing in order to observe the internal flow fields or by using complicated and expensive non-intrusive instruments. Comparison between the single-phase performance curve with multistage performance curve would give an idea about how significant the multistage performance degredation is considered to be. [7] mapped rough inflection points on every performance curve with the flow pattern transition for gas/liquid two-phase flow. Fig. 3 illustrates the pump pressure increment with respect to normalized liquid flow rate for single-phase as well as multi-phase flow [3].

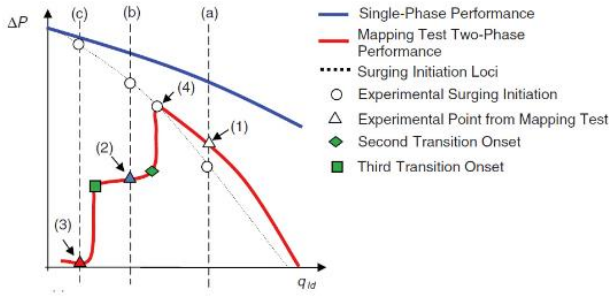

Figure 3: Multi-phase flow pattern investigation through interpretation of performance curves [7]

Various markers on Fig. 3 represent different inflection points on each one of the mapping test performance curves that is corresponding to dissimilar flow pattern transitions. The white circles represent the transition boundary between the dispersed bubble and bubbly flow. Fig. 3 provides a rough prediction on how detrimental multistage flow performance can be; furthermore, compared to single-phase flow, multiphase flow suffers a significant pressure degredation as the flow rate drops [3].

1.2 ESP Selection

Generally, ESPs are categorized into three distinct categories known as radial, mixed and axial type based upon their dimensionless specific speed, N_S as per Equation 1.

$$N_s = \frac{\omega Q^{\frac{1}{2}}}{(gH)^{\frac{3}{4}}} \quad (1)$$

There are a number of variables that need to be taken under consideration when choosing a submersible pump, such as efficiency, pumping head and brake horsepower. This allows picking the correct pump in augmenting the success of the system. Knowing the application for ESP is the first task is in selecting one; once known, the maximum discharge flow must be determined and emphasis must be given to the maximum discharge pressure of the pump. Lastly, ESP discharge size needs to be evaluated which will provide a reference to the size of discharge or the outlet connections of submersible pump [8].

Generally, submersible pumps are classified into two categories, known as the well pump which is suspended in liquid well on a pipe and are powered by AC voltage. Examples of well pumps include the electrical submersible pump, bladder pump, borehole pump and the line shaft turbines. The second category of pump is known as the sump pump which are utilized in smaller areas, such as a swimming pool or a pit. Examples of sump pump

include the grinder pumps, effluent pumps, the utility pump and bilge pump [8].

In case where ESP utilizes more than one impeller, it is known as a multistage centrifugal pump that contain multiple impellers located on same or different shafts. Multistage pumps provide more pressure and results in an increased output. Since ESP systems can work with a variety of flow rates and depths, they are in fact well suited for working inside oil wells by decreasing the well pressure at the bottom enabling large amounts of oil to be extracted [8].

1.3 Pump Head Analysis

Pump head refers to the pumps ability to transport fluid at different height or to transport fluid to different distances. Pump head can be written in formulation as per Equation 2 [9]:

$$\frac{h_P}{\gamma} = \frac{P_d}{\gamma} - \frac{P_S}{\gamma} \tag{2}$$

Pumps face pressure loss in the diffuser and impeller during pumping of a viscous fluid due to several factors, such as frictional loss, shock loss, leakage loss, recirculation loss, diffuser loss and disk loss. Taking the mentioned losses and deducting from the pump head can be formulated as per Equation 3:

$$H = H_E - H_{friction} - H_{shock} - H_{leakage} - H_{circulation} - H_{diffuser} - H_{disk} \tag{3}$$

where H is the pump head, H_E is the Euler head, $H_{friction}$ is the head loss due to friction, H_{shock} is the head loss due to shock, $H_{leakage}$ is the head loss due to leakage, $H_{circulation}$ is the head loss due to recirculation, $H_{diffuser}$ is the head loss inside the diffuser, H_{disk} head loss due to disk. Frictional effects generally become significant during high flow rate and the leakage is prominently at lower flow rates [3].

1.3.1 Euler Head

As an impeller rotates in a pump, fluid gets heaved into the blade passage at the center of the impeller known as the impeller eye. As fluid flows, it obtains energy from the impeller and while flowing through it, it gets discharged with an amplified pressure and velocity converting the kinetic energy into pressure energy. A centrifugal pump contains guide vanes at the inlet, and an impeller inlet angle that is designed in a way to develop a right-angled velocity triangle at the inlet as shown in Fig. 4. Assuming that the flow does not flow in the direction that it was designed to flow in, the direction of relative V_r will not coincide with the blade and the fluid shifts direction upon entering the impeller. This would cause eddies to rise and give rise to back flow in inlet pipe. The Euler pump head that formulates the performance curve can be determined conferring to ideal conservation law of angular momentum as per Equation 4 [3]:

$$H_E = \frac{V_{w2}U_2 - V_{w1}U_1}{g} \tag{4}$$

where H_E is the work done on fluid per unit weight and g is acceleration due to gravity; Equation 4 refers to the difference between projection of absolute velocities at impeller inlet and outlet. Observing Equation 4 highlights that work done is autonomous of inlet radius, and difference in total head across the pump is defined as manometric head. This head is generally considered higher than actual difference in elevation between the inlet and outlet points.

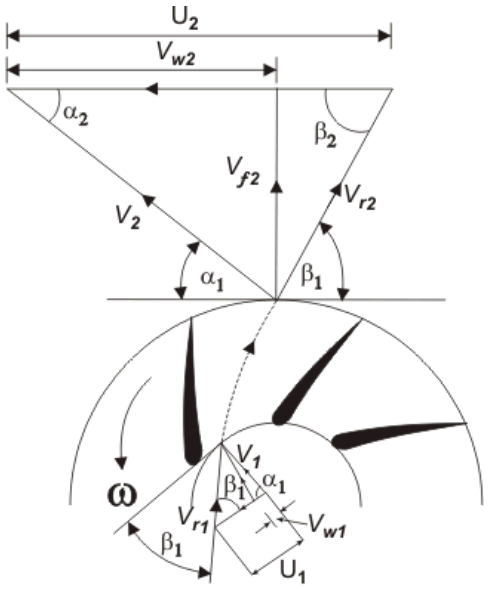

Figure 4: Velocity Triangles for centrifugal pump impeller [3]

1.3.2 Frictional Losses

Frictional losses progressively grow with liquid flow rate and are caused by fluid friction in impeller. The term pressure drops or pressure loss is often used to refer the decrease in system pressure due to friction. The friction losses are discovered for energy dissipation caused by contact between the fluid with solid boundaries, such as stationary vanes, impeller, casing, disk and diffuser etc [10].

According to [11] , the head friction loss can be obtained using Equation 5.

$$H_{friction} = \frac{f_{\gamma\beta\omega} Q^2}{8 g D_H \pi^2 {b^2}_m \sin^3 \beta_m} \frac{r_2 - r_1}{r_2 r_1} \quad (5)$$

[10] calculated frictional loss in impeller through MATLAB while the varying the geometry of the impeller and analyzing the curves which illustrated that head loss in impeller increases with respect to flow rate.

[12] measured the effects of surface roughness on pump performance at low specific speeds using Numerical Simulations as well as verifying the results through prototype. It illustrated that most of the losses originate from the volute and the side chamber flow highlighting that the assumption of hydraulic smooth walls in industrial pump simulations were incorrect.

[13] strained to improve the head friction losses through theory and experiment in laminar flow, and ended up altering the friction coefficient as per Equation 6 which is for both the smooth round tubes and rectangular ducts.

$$\frac{1}{\sqrt{f}} = 2.0 log_{10} Re^* \sqrt{f} - 0.8 \quad (6)$$

[14] found out that friction loss coefficient that is appropriate for all Reynolds number and for all surfaces by uniting all equations together and simplifying them into one equation that will be suitable for all flow regions and surfaces. The combination of equations provided a reasonable error which resulted in the friction coefficient being represented in Eqs. below which is valid for all *Re* and $\in/D$.

$$f = [(\frac{8}{R_e})^{12} + \frac{1}{(A+B)^{\frac{3}{2}}}]^{1/12} \quad (7)$$

$$A = [2.457 \, ln \frac{1}{(\frac{7}{R_e})^{0.9} + \frac{0.27\epsilon}{D}}]^{16} \quad (8)$$

$$B = (\frac{37530}{R_e})^{16} \quad (9)$$

[15] developed another head friction loss model represented by Equation 10. Their study also mentions many losses including friction loss that are involved in pressure loss across the pump.

$$H_1 = \frac{b_2 (D_2 - D_1)(W_1 + W_2)^2}{2 sin\beta_2 H_r 4g} \quad (10)$$

According to [15], the frictional losses are due to contact between the solid boundary including all the parts that contact with the fluid.

Blade loading loss is one of the frictional losses that occur due to pressure difference between the pressure and suction side of the blade. According to [16], it accounts for the blade-to-blade pressure gradient that generates a secondary flow that leads to stall; it can be calculated using Equation 11.

$$\omega_{bl} = \frac{(\frac{\Delta W}{W_1})^2}{24} \quad (11)$$

Mixing loss occurs due to the mixing of blade wake flow with free stream flow. The wake mixing loss can be calculated using Equation 12 [13].

$$\omega_{mix} = [\frac{C_{r,wake} - C_{r,mix}}{W_1}]^2 \quad (12)$$

Clearance loss occurs in the pump between the blades and the casing when some flow that is exits the impeller leaks through the clearance gap and caps to the lower pressure region of the compressor. The clearance loss can be calculated using Equation 13 [16].

$$\omega_{cl} = \frac{2 \dot{m}_{cl} \Delta P_{cl}}{\dot{m} \rho_1 {W_1}^2} \quad (13)$$

1.3.3 Shock Loss

Shock losses are generated at the entrance and exit of the impeller due to sudden changes in direction of flow; however, pump functioning at Best Efficiency Point does not experience shock losses. Flow rate that differs from the designed flow rate will cause major shock loss. According to [15], shock loss occurs due to differences between flow and metal angle at the inlet impeller that can be formulated using Equation 14 which is effective for all Re within the flow rate range of the pump. Thin, Khaing and Aye also provided a relation between Flow rate, Q and the H_{shock} as shown in Fig. 5. Observation of the graph illustrates that a decrease in flow rate provides an increase in shock loss accordingly. Shock losses does not take design point

into consideration and elimination of the condition results in a higher shock loss [15].

$$H_s = K(Q_S - Q_N)^2 \tag{14}$$

[3] studied the effect of changes in flow direction once the flow exits the impeller and enters the diffuser; whereas it was opposite for the next stage causing turns loss or shock loss. Shock loss can also be calculated using the shock component as per Equation 15.

$$H_{shock} = \frac{\tau_{shock} W_{shock}^2}{2g} \tag{15}$$

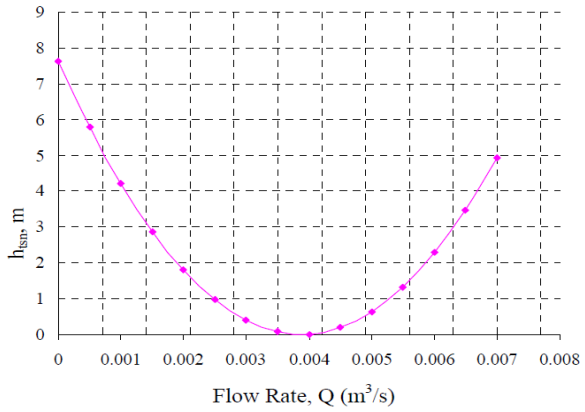

Figure 5: Head loss due to shock vs Flow rate [15]

1.3.4 Leakage Loss

Leakage losses characterize loss of liquid flow rate through clearances between rotating and stationary components of a pump [17]. These leakages can be prevented through implementation of specific design parameters that are adequately met along with emission requirements. Generally, the seal face leakage depends on the pump motor operating conditions. If functioning vibration levels are significant; then shaft suffers extreme radial and axial movement. According to [18], pump leakage occurs due to the distinction between outlet and inlet pressure of impeller where a portion of the impeller outlet flow rate, Q_L, returns back to the impeller inlet from the existing clearance between the impeller and the casing. According to [19], leakage loss can be formulated as per given Equation 16 which is valid for all Re.

$$H_{lk} = \frac{Q_{lk} U_{lk} U_2}{2Q * g} \tag{16}$$

Typically, the seal leakage occurs from the sealing interface. While in some situation's leakage can come from the secondary sealing area like O-rings, this happens due to O-ring degradation dependent upon the substance flowing in the pump. In some cases, the sealing rings are porous and the fluid tends to leak through the bodies. These leaks can be predicted for seal with a given pressure difference across the seal. Typical total pressure drops, ΔP can be calculated from the seal inlet chamber to the exit chamber using Equation 17 [20].

$$P_s - P_e = \frac{\left(\xi + \xi_e + 4f\left(\frac{L}{2C}\right)\right)\rho W^2}{2} \tag{17}$$

1.3.5 Recirculation Loss

[19] studied recirculation loss and defined it as the loss that occurs due to adverse pressure difference between the inlet and the outlet of the impeller; furthermore, the recirculation loss increases once the liquid flow rate decreases as the pressure gradient decreases according to the flow rate. The recirculation loss can be formulated in Equation 18.

$$H_{rec} = \frac{f_{rec}\left(\sinh(3.5\alpha^2)\, D_f^2 v_2^2\right)}{g} \tag{18}$$

where V_2 is the average circumferential velocity at the impeller outlet.

According to [15], the coefficient of recirculation loss is a function of the piping configuration or the geometry of the inlet. Recirculation power can be converted to parasitic head by dividing the volume flow rate as per Equation 19.

$$H = K\omega^3 D_1^2 \left(1 - \left(\frac{Q_s}{Q_1}\right)\right)^{2.5} \quad (\text{when } Q \leq 0.0025 \tfrac{m^3}{s}) \tag{19}$$

If K is assumed to be 0.005 the head loss will be zero since $Q \geq 0.0025 \frac{m^3}{s}$. Fig. 6 provides an illustration that at low flow rates the recirculation loss tends to be high for large impeller diameters; however, it is negligible at high flow rates. The recirculation loss occurs inside the impeller due to the shear effect which depends upon the fluid viscosity, the geometry of the impeller channel as well as the shear velocity [15].

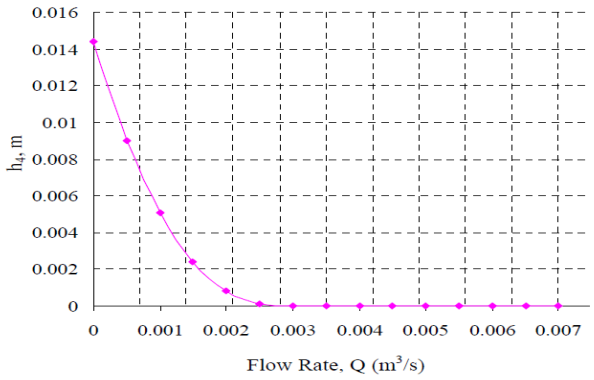

Figure 6: Recirculation loss vs the flow rate [15]

1.3.6 Diffuser Loss

Disk losses occur due to interaction amongst the fluid and the rotating disk. These acquaintances allow the pump to consume additional power in order to rotate the disk that is delayed by viscous shear forces present in the fluid. These disk losses are caused due to mechanical losses formed in flowing group, but the model is still father away from being substantial. [15] highlighted that once the disk losses are proportional to the fifth power of disk radius as shown in Equation 20, then the friction coefficient would intensify with increasing angle of the developed outlet section of disk.

$$H_{disk} = \frac{f_{disk}\rho\omega r_2^5}{10^9 Q} \tag{20}$$

[21] derived the torque by the rotating radial disk as shown in Equation 21 below.

$$M_{df} = \int \tau r dA \tag{21}$$

Once Equation 21 was formed which relates the shear stress, the friction coefficient was replaced with E_c empirical constant, the final Equation 22 and Equation 23 were formed.

$$M_{df} = \frac{1}{2}\rho\omega^2 E_c r^5 \tag{22}$$

$$E_c = \frac{2}{5}\pi C_f \tag{23}$$

Furthermore, a widespread study conducted on a rotator fisk showed the limitations and the validity of Equation 23. Four conceivable commands were distinguished and were valid for different limitations of E_c:-

- Regime 1: Laminar flow through small clearance
- Regime 2: Laminar flow through large clearance
- Regime 3: Turbulent flow through small clearance
- Regime 4: Turbulent flow through large clearance

[22] and [23] presented a prototype of disk loss as a function of geometry that included the shape of the impeller (f_{rs}), friction factor (K_{RR}) and gap among the impeller and casing (h).

$$H_{disk} = \left(\frac{K_{RR} f_{th}\omega^2 r^5}{gQ}\right)\left(1 - \left(\frac{D_1}{D_2}\right)^5\right) \tag{24}$$

$$K_{RR} = \frac{\pi r_2}{2R_e h} + \frac{0.02}{R_e^{0.2}}\left(\frac{\left(1+\frac{h}{r_2}\right)}{1+\frac{h}{2r_2}}\right) \tag{25}$$

$$f_{th} = \exp\left(-2 * 10^{-5}\left(\frac{v}{10^{-6}}\right)^{1.34}\right) \tag{26}$$

where $h = 0.05 r_2$.

The Equations above state that at viscosity above $40 \times 10^{-4}\left(\frac{m^2}{s}\right)$ the fluid will heat up and will be notable. Once the viscosity reaches 9.1×10^{-4}, the friction factor will be only about 75% of the predicted values.

All the above losses are still considered in centrifugal pump flow. The normal head developed by the impeller considering ideal operating conditions are calculated from the increase of centrifugal force acting on the liquid contained between two successive vanes assuming that there are infinite impeller vanes; However, in reality, impeller vanes are limited and the liquid that is contained between the two vanes develops a circulating flow which modifies the velocity distribution as well as the theoretical head developed as shown in Fig. 7, which provides an illustration of all head losses represented by a *H-Q* curve [24].

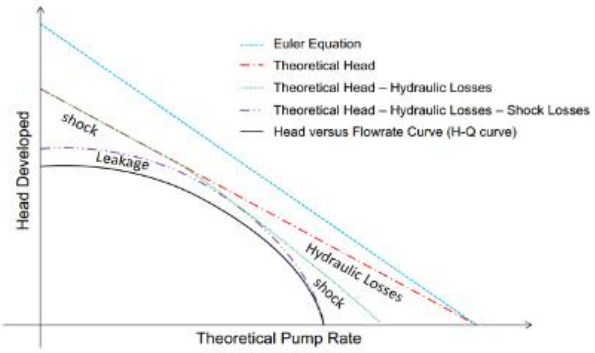

Figure 7: Theoretical and Actual head comparison with respect to the flow rate [17]

1.3.7 Losses in Industry

These losses are faced in the industry at a much larger scale. Engineers are obliged to design instruments in order to measure these losses and eliminate them. This study looks at how the losses are measured at an industrial scale. Frictional losses or more specifically disk friction loss is measured using thin plain disk with a constant thickness that rotates in a close-fitting and close casing. Most pumps have their hub and shroud surfaces not radial and not complete; however, some papers have discussed that disk friction loss formulae include the impact of both the outside surface roughness of the hub, shroud and the casing. Most traditional published articles have not reviewed the losses in pumps if the specific speed or the size of the pump were to be altered [25].

New concepts for measuring disk friction loss utilize one-dimensional theory of turbomachinery, through experimentation work, the pump and the solid disk being tested are to be coupled to a constant speed A.C electric motor through a torque meter that aids the measuring of the torque that is transmitted along with a special speed sensor for measuring the rotational speed. The net power loss is measured through taking a difference between the power measured when the casing is filled with water and the power measured when the pump casing was empty. This would exclude the bearing loss in the net power loss. For power measurement inside the pump, apparatus, such as the hub-type torque meter and the Disc-type torque meter that are installed between motor and pump or between gear and pump respectively [25].

There are several ways to detect leaks, such as the spark coil technique. This technique uses a high voltage or Tesla cod as well as sparkling point in order to create the electromagnetic radiation that causes the generation of glow discharge in the neighboring evacuated ampoules. Once the leak is drawn into the antenna, plasma can be observed inside and travelling towards the leak; however, there are certain drawbacks, including radio disturbances. Another method to measure the leakage is the Pressure change method that utilizes pressure gauges which are the ordinary once used to measure the system performance. Let's say there is a leak, the leak site can be squirted with a solvent like acetone and watching the gauge for the pressure rise that occurs once the solvent enters the leak. Another method can be the Overpressure method that uses liquid and gas with which the element being tested gets filled. Testing with gas, the vessel gets subjected to overpressure of some bars and then immerged into water. At the leaks, gas bubbles start to escape and a leak up to 10-3 mbar/s can be detected. Let's say the vessel is too large for the immersion then the points must be painted by the soap solution and the bubbles will be visible once again. This method is generally used for large systems [26].

Generally, at low flow rate, flow separation occurs causing instability in the flow making the pump perform worse [27]. High incidence angle causes spikes due to the flow separation at the impeller leading edge and vortices appear at the blade suction side moving towards the pressure side. At the same time, it will be towards the casing [28]

2 How Single Phase and Multi-Phase losses are compared with each other?

Above literature provides explanation on single-phase flow and the losses associated with it. But how do multi-phase losses compare to the single-phase ones. Multiphase flow impacts turbomachines operation introducing secondary flows, unsteady phenomenon as well as other disturbances in the flow field. Single-phase doesn't contain any bubble unlike multi-phase where the flowing liquid has bubbles in it. There are different design variations for a helicon axial multiphase pump which depends on the function of GVF and the inlet pressure. Using preliminary induces would make sense in order to reduce the bubble size which causes chocking and shock losses when operating at a low suction pressure [29].

A method developed by Korenchan was based on calculating the head ratio between two-phase and single-phase head losses. In order to calculate this, the difference between the theoretical and the actual performance must be calculated for both the single-phase and the two-phase. The head loss ratio can be calculated using Equation 27 below [30].

$$H^* = \frac{\psi_{TP,th} - \psi_{TP}}{\psi_{SPL,th} - \psi_{SPL}} \quad (27)$$

where ψ refers to the head coefficient

According to [31] the pump operating at 15% GVF would consume slightly more power as the inlet pressure decreases and this is due to condensed parting of liquid and gas phase in the major separator and the as the pressure surges causing an increase in gas entrainment in liquid flow.

3 Multiphase Flow

Multi-phase flow is a general phenomenon that arises not only in the oil and gas industry, but correspondingly in the chemical and the nuclear industry as well [32]. Multiphase applications that include the transport of LNG cause operational challenges in the form of air bubbles that present cavitation as well as degradation risks to the major components of the pump. LNG is basically natural gas that is converted into liquid form for ease of transport as liquids take way less space compared to gas. The process of cooling the natural gas into liquid is known as liquefaction after which the liquid LNG has to be converted back into gas for applications. In an LNG liquefaction plant, once natural gas has been cleaned of its impurities, its methane form gets converted to liquid through a refrigeration technology which cools the gas down to about -162°C which is where the two-phase flow gets generated. During transportation of LNG, some liquid gets boiled off into gas and that gas is utilized as a supplement for fuel [33].

Industries utilize Two-phase LNG expander that transforms the hydraulic energy gained from the pressurized fluid to kinetic energy and then later to mechanical power input which finally gets converted to electricity. In LNG industry, the traditional liquefaction process operates at a higher pressure through the condensation phase after which the pressure dies down once it passes through the expansion valve. The design of most expanders that are being installed in the industry right now are so carefully designed that if vapor breaks inside the expander; the machine is able to tolerate it. It is kept at a backpressure of about 5 bars above the liquid bubble point in order to make sure LNG remains in its liquid form [32].

Generally, in the industry, two phase flows cause instabilities in LNG mixture flowing through pipelines. Once LNG begins to vaporize, it starts to expand quite rapidly as shown in Fig. 8. Closer to the boiling point, LNG increases by approximately 150 times its original volume for every 1°C increase in temperature. For a terminal containing a long pipeline, this can cause a number of problems in the industry or in other words can cause instabilities. Some instabilities include the density-wave-type, pressure-drop-type and the thermal type oscillations in a single-channel up flow boiling system [34].

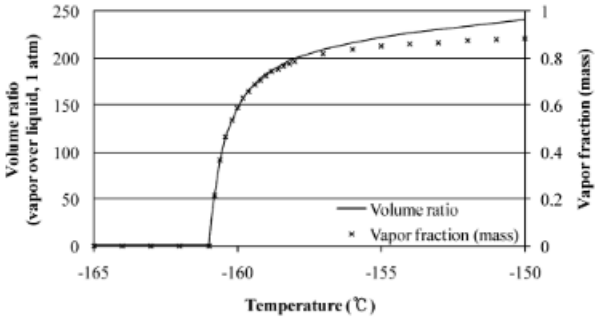

Figure 8: Ratio of volume or vapor fraction increase with respect to temperature [34]

From visualization analysis and experiments of phase distribution present in the impeller and the diffuser, four common flow patterns were recognized. Three of the four patterns were identified by [35], namely the bubbly flow, agglomerated flow and gas pockets. According to [1], an annular flow pattern is observed at very low liquid flow rates. These flow patterns vary according to flow rates, fluid properties as well as geometrical variations. Two-phase flow can also be divided into two classification, such as continuous flow and discontinuous flow. Once one of the phases does not interfere with the other phase then a continuous flow is maintained, otherwise it's a discontinuous flow. None of the previous literature discussed the effects of detailed flow structures on the losses mentioned above, while this paper investigates the vorticity patterns as well as the vortical activities due to the interactions between the bubbles and flow.

3.1 Bubble Flow

Bubble flow is generally an unremitting flow of liquid at a relatively high flow rate and low gas volume fraction with small gas bubbles. In centrifugal pumps the gas flows in terms of dispersed bubbles through the continuous field as shown in Fig. 9. Little to no interaction between the bubbles is observed [1] along with no apparent aggregation of the dispersed phase. Smaller bubbles have a spherical shape while the larger ones are observed to have an irregular one [35]. Observing the impeller, bubble flow is very well-oriented with the blade geometry; however, it is close to the

impeller outlet that gets bounced towards the pressure side prior to exiting the impeller [1]. The gas flow impacts the number of bubbles formed in the impeller, whereas the rotational speed of the impeller and liquid flow rate determine the bubble shape and size [35].

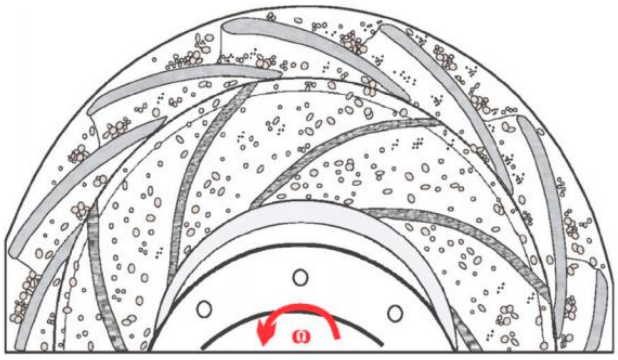

Figure 9: Bubble flow at the impeller and diffuser [1]

Generally, bubble size tends to decrease as the rotational speed of impeller increases due to the intensification in drag forces and turbulence intensity. This flow does not contain a high intensity of gas accumulation and that is due to the drag force being adequate enough to carry the gas along with liquid disregarding the centrifugal field produced by the pump's rotation [35]. This flow pattern showed pump performance close to the single-phase flow with less than 8% performance degredation in terms of pressure-rise [1].

In bubble flow patterns, measurements are taken for the air bubbles. A typical measurement taken for bubbles is their diameter, and it is defined as the diameter of the sphere whose shape the bubble accumulates. Generally, all bubbles do have a prolate spheroid shape which is retrieved through revolution of an ellipse. At higher gas volume fractions, it is quite difficult to make out the bubble shape [35].

3.2 Agglomerated Bubble Flow

This flow pattern tends to occur for large gas volume fraction and those that are related to bubble flow [1]. Once the gas fraction increases, bubble population increases as well, and so do their sizes as shown in Fig. 10. As the population increases, the space between the bubble decreases, increasing the amount of interaction between them [35]. This interaction between the bubbles lead to the formation of larger bubbles unlike the bubble flow; It also increases the sparse spots of gas coalescence, which proceeds to form small gas pockets that have irregular shapes that are continuously deforming or broken by liquid phase passage [1].

The continuous and dispersed phase in this flow are water and air. Drag force is not sufficient enough for carrying the deformed bubbles with liquid. The adverse pressure gradient generated within the impeller slows the air bubbles down [35]. In addition to that, intense bubble recirculation can be observed together with intense liquid phase turbulence in the impeller channels [1].

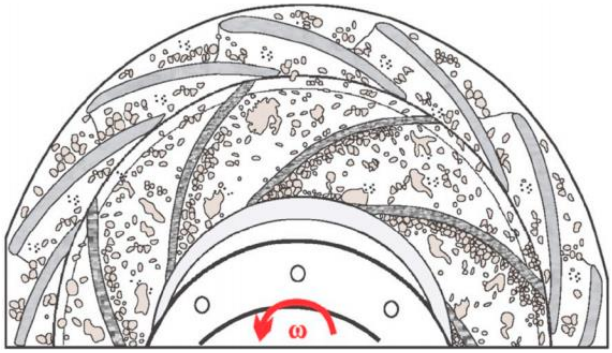

Figure 10: Agglomerated Bubble flow at the impeller and diffuser [1]

3.3 Gas Pocket

Gas pockets occur once the gas volume fraction is increased further from agglomerated flow [1]. First observation is the coalescence of bubbles increases which results in larger bubbles. This increase in bubble size diminishes space at the impeller channel by constraining the accessible area for liquid flow [35]. The diffuser channel faced an increase in bubble population unlike the impeller channel [1]. The-gas liquid interface is intensely deformed as well as unstable which provides an indication that the flow is instable as shown in Fig. 11 [35].

Either it be the stable or the unstable gas pockets, both accumulate a small portion of bubble in the wake created downstream of pocket [1]. This region gets accumulated by bubbles that have detached from its main structure and have formed an intense recirculation region. The impeller area that is blocked by the gas pockets diminishes the amount of transference of kinetic energy into the liquid which decreases pumps own capacity in order to develop pressure as well as add instability to the pump operation. The operational instability that originates from this flow is known as surging [35].

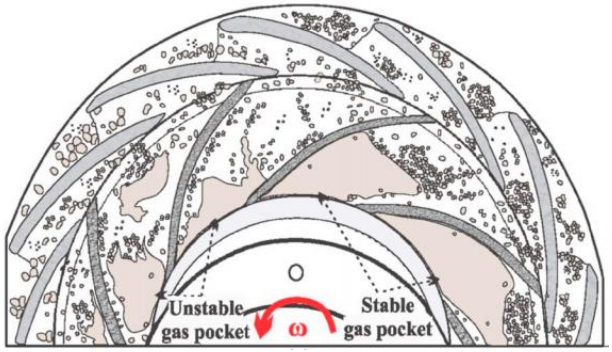

Figure 11: Gas pocket at the impeller and the diffuser [1]

3.4 Annular/Segregated Flow

Annular flow is generated at low liquid flow rates, and this flow pattern is detected only at the impeller channels whereas only a small dense dispersion of small sized bubbles is observed at the cross-section of the diffuser channel. This flow contains stable pockets and inhabit the whole cross-section of the impeller channels as shown in Fig. 12. It is easier to understand in the way that gas phase deviates from the liquid phase and forms a continuous phase that stays fixed through the impeller inlet and outlet forming an elongated bubble. At the impeller inlet, a zone comprehending strong coalescence amid the gas pockets and the dispersed bubble crosses the threshold through the suction pipe. At the impeller channel outlet, gas pockets trailing surface gets fragmented continuously constructing a wake region downstream with a dense dispersion of small bubbles [1].

The reduction in useful area for the liquid to flow, the pump is incapable to transfer enough energy to the fluid leading to a near zero head. This situation is named as Gas locking, which is a functioning problem throughout the industry inclined not only by the pump but by the complete pumping system. It is represented as a function of various flow parameters, such as properties of fluid, geometry of pump as well as installation characteristics. In Oil well applications, as soon as the reservoir contains no adequate amount of pressure in order to promote the fluid flow, gas locking conditions does not only promote null pump head, but also causes null flow [35]. Some relevant study can be found in [48].

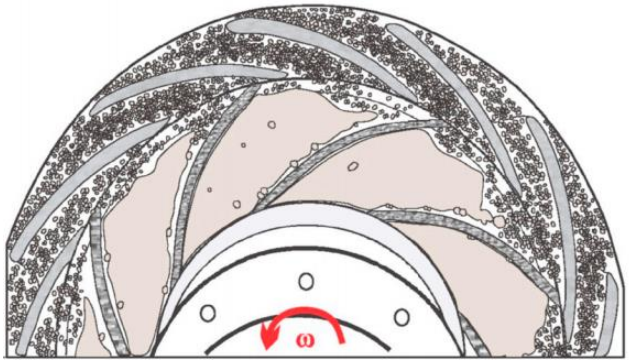

Figure 12: Annular flow at the impeller and the diffuser [1]

3.5 Flow Pattern Maps

Flow pattern maps are normally created with liquid superficial velocity on the y-axis with respect to gas superficial velocity on the x-axis. These maps encompass of experimentally determined flow pattern that are plotted with numerous indicators and boundaries. Determining the flow pattern that occurs in the flow requires knowledge of certain variables, such as gas and liquid properties, pipe geometry and the gas and liquid superficial velocities. These flows are generally defined for pipe flows, such as Fig. 13 illustrates the Baker map that is an example of flow pattern map for horizontal flow in a pipe.

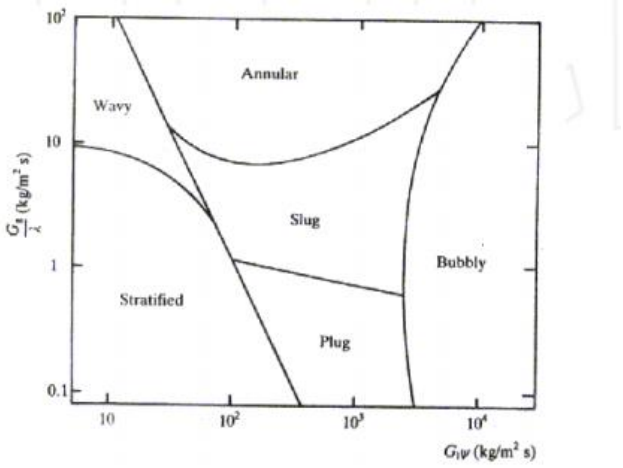

Figure 13: Baker flow pattern map marking the horizontal flow in pipe [36]

Unlike the above flow pattern map, the Beggs and Brill relationship necessitates classifying the flow pattern at a given flowing condition so as to compute the liquid holdup along with the friction. The Beggs and Brill correlation inclines to make use of the horizontal flow pattern map that is constructed on the basis of Froude number for the mixture and input liquid content. Fig. 14 illustrates the flow patterns that are grouped as segregated, intermittent, distributed and transition flow [37].

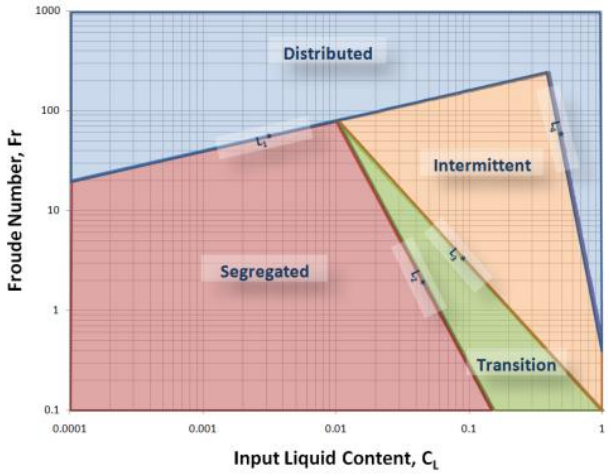

Figure 14: Flow Pattern map for horizontal pipe [37]

4 Two Phase Performance Curve

Two-Phase flow in general deteriorates the pump performance by an enormous amount. For observing the head deterioration of pump once gas volume fraction is introduced. Jhoan [1] experimented on two phase flow in order to understand the effect of rotating speed on the bubble diameter. The flow rate and gas volume fraction were fixed at 1.5 and 2% respectively, for three different impeller rotating speeds of 300, 400 and 500 rpm. They formed a graph plotting the two-phase flow at different impeller speeds alongside single-phase flow for comparison as shown in Fig. 15 below. The head degredation at lower flow rates is shockingly high, but it increases as the rpm increases. 300 rpm showed a less than half the single-phase flow head degradation at Gas Volume Fraction of only 2% [1].

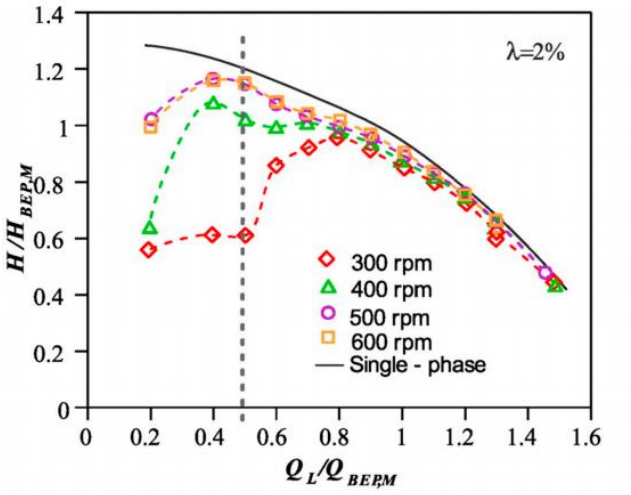

Figure 15: Stationary head curves at 2% continuous no-slip gas volume fraction [1]

5 Experimental Studies to develop performance curve on ESP

Since very low literature is available on the topic of two-phase flow visualization in an Electrical Submersible Pump, most researchers are trying to visualize the flow using high speed cameras and transparent casings; whereas some are trying to simulate the problem in order to predict the flow pattern inside the pump.

5.1 Single-Phase Flow Experiments

Generally starting off with simulations, the first step in a research is to verify the model which in this case can be done by corresponding to the simulation performance curve with performance curve provided by the manufacturer and try his best to follow affinity laws since most of the pumps and experiments that are modified depending on what the conditions are at hand. [38] modelled a specific pump design in ANSYS for two-phase flow simulation, their CFD model comparison with the provided catalogue performance curve is shown in Fig. 16. Their numerical pump boosting pressure matched well with the provided curve with an average discrepancy of 5% validating the numerical model for further study.

[39] verified another pump model for CFD calculations in order to observe the general performance, like efficiency and pumping head. Fig. 17 shows the comparison between the simulation results and the manufacturer curve, and their simulation results tend to be slightly higher than theoretical due to smooth wall assumptions that were set beforehand; however, their simulation results showed a consistent downward trend as the liquid flow rates increased [39]. Most researches provide a mesh independency graph for understanding the mesh validation at the Best efficiency point, such as simulating the pump design at its BEP flow rate as per the manufacturer and changing mesh elements as per the computational power. Ranging from 1 million to 9 million mesh elements would illustrate the best mesh element size that must be selected for the given model as per the computational power available and time taken per simulation. As the mesh size reduces or as the mesh becomes finer, the errors in numerical solutions tend to go down. As the number of meshing grids surges the simulated pressure increment diminishes.

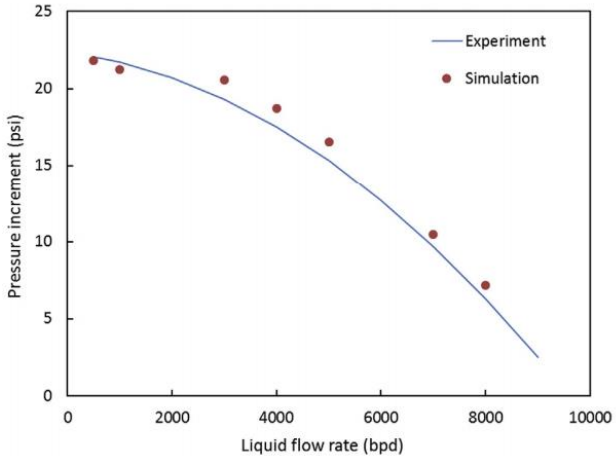

Figure 16: Comparison of Numerical Simulation results with actual performance curve at 3600 rpm [38]

[40] simulated another pump design that also included the two-phase simulation and experiment results for error comparison as shown in Fig. 18 below. It provides an illustration of pump head with respect to the flow rate at an impeller rotation speed of about 3000 rpm. Their simulation results came out to be slightly higher than expected due to flow conditions that are ideal to the real flow and it is quite difficult to predict leakage loss in numerical simulations.

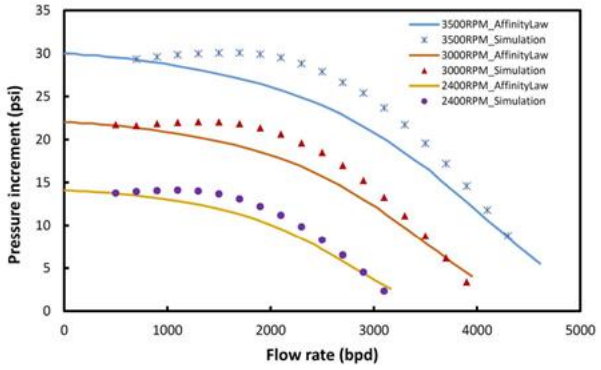

Figure 17: Comparison between numerical simulation and actual pump performance curve for TE 2700 ESP [39]

The difference or error in the values was not apparent, but the difference surges with respect to the flow rate. The three-stage pressure increment showed a maximum error percentage of 10% when compared to the experimental performance curve; However, the error is within acceptable range and can be considered acceptable for further investigation [40].

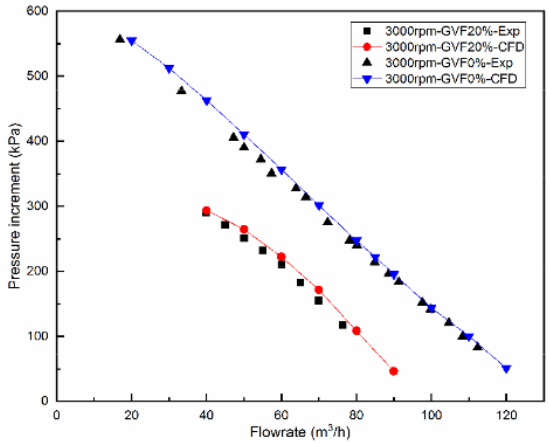

Figure 18: Comparison of Numerical results with simulation results at 3000 rpm [40]

In terms of multiphase models, the Eulerian-Eulerian approach has three dissimilar Euler-Euler models that are available, such as the Volume of Fluid method (VOF), the Mixture model and the Eulerian Model [41].

The VOF method is the most famous method for volume tracking and locating the free surface. Most models generally use a single set of transport equations, and it is model so that two or more immiscible fluid solve a single set of momentum equation while tracking the volume fraction of each fluid throughout the domain. The VOF method contributes reliability and effectiveness and has been updated throughout the years. This method is easy to extend into a 3-Dimensional space and simple to implement; However, it lacks simplification of its linear terms in equations and in some cases, it can lead to less accurate solutions [41].

Mixture model is basically a simplified multiphase model that is utilized for different scenarios. It can be used to model homogeneous multiphase flow as well as to calculate non-Newtonian viscosity. It solves the energy equation for the mixture. The mixture model has its own pros, such as the minimum number of variables that are to be solved. It basically reduces the computational time. It requires less memory and disk space; however, in complex problems the solution becomes non-Newtonian [41].

The Eulerian model is by far the most general model that solves multiphase flow problems, but it also contributes to the most complex model of the three. It treats all the other phases as continuum basically solving the continuity, momentum and energy equations. Some of the eulerian applications include bubbly flow, risers, fluidized bed. This method provides much

accurate results; however, it requires more simulation time compared to VOF and mixture methods [41].

5.2 Two-Phase Flow Experiments

[42] were the first ones to investigate the effects of air bubbles in centrifugal pumps. Through their research, they observed that air bubble entrainment at the impeller causes a continuous pump performance degredation as the gas volume fraction increases. As time moved on, pumps started to contain more components than usual with more complexity. Observing gas entrainment in modern Electrical Submersible Pumps is challenging with little literature review on the topic. [1] researched further into the performance degredation and provided insightful information for future literatures.

[1] took two-phase flow images using a high-speed camera and broke them down one by one with each flow structure. This report looks into a couple of the major flow structures that were encountered as shown in Fig. 19. Flow Structure 1 below provided a visualization of dispersed bubbles at the impeller as well as the channels with insignificant agglomerations and coalescence. After passing the impeller channel the bubbles move to the pressure surface due to influence of lateral pressure gradient. Since this pattern did not experience agglomerations and coalescence, it showed negligible head degradation [43-47]

Flow structures 2 and 3 were similar to flow structure 1 with only change being in the bubble population and size. Observing flow structure 4 the bubble agglomerations and the coalescence increased at the impeller channel inlet. Observation from a couple channel showed development of gas pockets which as are unstable in nature; However, some channels remain unbothered by the gas pocket formation, but were only impacted by the bubble agglomerations. At the diffuser, bubbles flowed through the entire channel cross-section along with a population that is greater than Flow structure 3 [1].

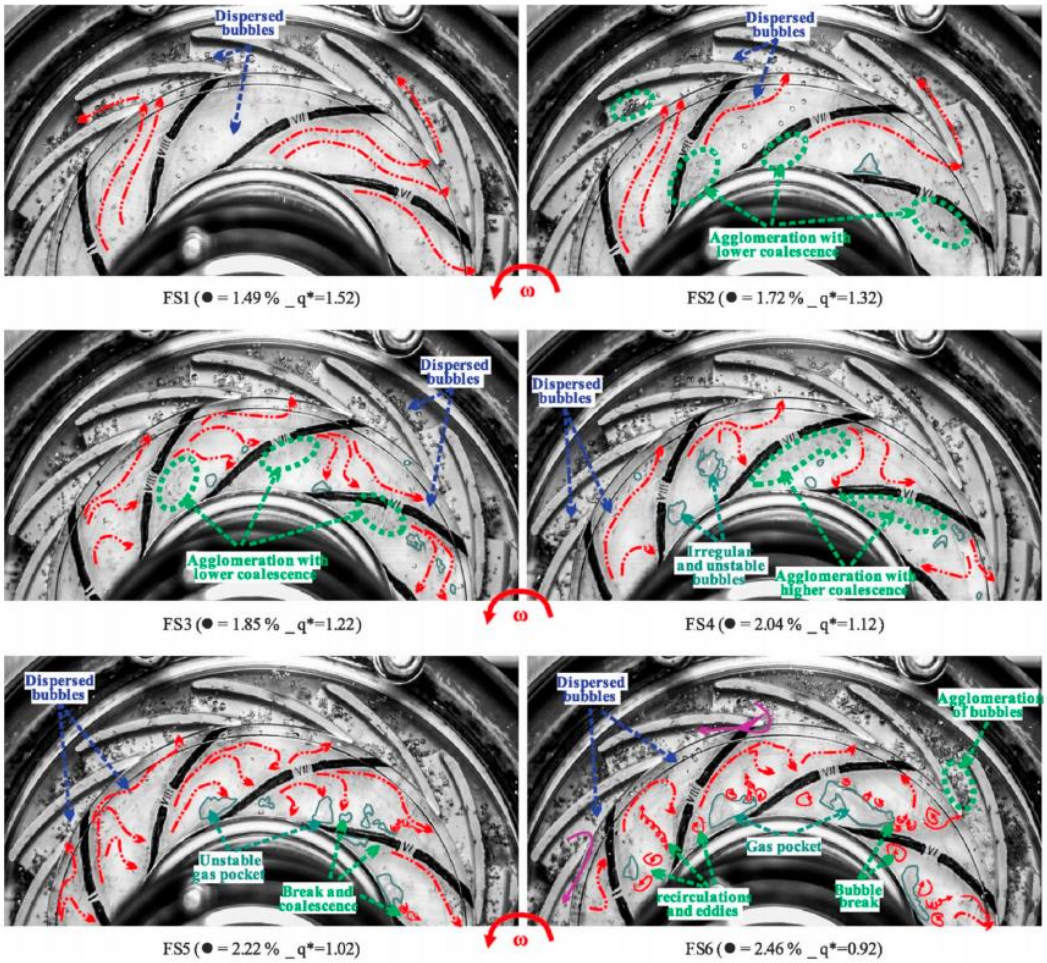

Figure 19: Two-Phase flow structures for a fixed rotational speed of 300 rpm and constant air flow [1]

At flow structure 5 majority of the channels starting experiencing gas pocket formation hinting that bubble coalescence will start to influence the gas phase distribution significantly. Gas pockets are

larger than flow structure 4 being more unbalanced and continuously sheared by the liquid phase. Bubble recirculation grows greater inside the impeller channel. An observation of a balanced competition between bubble breakup and coalescence was noticed mostly related to liquid phase turbulence [1].

Finally, flow structure 6 showed significant increase in recirculation and bubble coalescence at the impeller channel inlet. Coalescence and bubble breakup continue; however, this time the coalescence take the lead at the channel inlet causing large size bubbles to form which are not completely broken. Right after the bubbles flow to blade pressure side, some bubbles flow back to the entrance which was not observed in previous flow structures. Gas pockets are formed halfway through the impeller channel as well as much closer to the impeller channels [1].

Through observation of the above flow structures, it can be noticed that the amount of pump head degredation is very closely related towards the flow patterns observed in the pump. The breakdown of flow patterns evaluates phase distribution as well as the bubble behavior patterns internally at the impeller and the diffuser. Operating conditions, such as the impeller rotational speed, the flow rate and the gas volume fraction greatly impact these behavior [1].

6 Recommendation and Conclusion

In conclusion, a number of researches investigated the performance degredation in ESP owing to introduction of two-phase flow as per the LNG and Oil and gas industries. This review of experimental and numerical simulation on ESP performance degredation has highlighted the complications behind accurately predicting the flow behavior of two-phase flow inside the pump. The turbulence flow along with transient behavior has made it challenging to observe the flow structures successfully. An alternate option is through numerical simulations; however, their reliability and validity is still in question due to the strong shearing effects. This review paper highlights four types of flow behavior namely, the bubble flow, agglomerated flow, gas pocket and annular flow. Each flow pattern has a different effect on the pump performance, such as agglomerated flow showed little to no impact on the performance while annular flow showed sever performance degredation. Further research into the ESP showed that an increase in pressure intake pressure resulted in a positive effect on the pump performance for two-phase flow.

This review provides a solid basis on the complications that impact the precise estimate of two-phase performance inside an ESP. Even though this paper emphasized more on the flow structure in an experimental setting of an ESP, CFD simulations is an alternative technique for observing multiphase flow, especially when other variables, such as wall shear stresses and phase interactions are taken into consideration. Future researches can focus upon further study of multiphase flow in terms of ESP head degredation due to wall shear stresses at the impeller blades or through the study of phase interactions which are not well understood.

ESP performance under two-phase flow still requires further research as there is always room for improvement on the prediction model:

- Observation of two-phase flow in multistage pump can provide answers to several questions as what would happen to the bubbles at the third or fourth stage of the pump; moreover, measuring the GVF is difficult and inaccurate resulting in difficulty characterizing the pump.
- Experimentation requires further development, as in using different fluids and gases rather than air and water. Would it provide the same deterioration; furthermore, improve capturing of two-phase flow at much higher GVF and various liquid flow rates to achieve various flow patterns.
- Numerical simulations require further improvements by reducing floating points based on rotational speed and minimum mesh length and providing comparison between various turbulence models for a better comparison on the accuracy of results.

References

[1] J. M. Cubas, H. Stel, E. M. Ofuchi, M. A. Marcelino and R. E. Morales, "Visualization of two-phase gas-liquid flow in a radial centrifugal pump with a vaned diffuser," *Journal of Petroleum Science and Engineering,* vol. 187, pp. 1 - 14, 24 December 2019.

[2] J. Zhu and H.-Q. Zhang, "Numerical Study on Electrical-Submersible-Pump Two-Phase Performance and Bubble-Size Modeling," in *SPE Annual Technical Conference and*

Exhibiton, Tulsa, 2014.

[3] H. Q. Zhang and J. Zhu, "A Review of Experiments and Modeling of Gas-Liquid Flow in Electrical Submersible Pumps," 11 January 2018.

[4] M. M. A. Klazly and G. Bognar, "CFD Study for the Flow Behaviour of Nanofluid Flow over Flat Plate," *International Journal of Mechanics* , vol. 14, pp. 49 - 57, 2020.

[5] A. Giniatoulline, "Mathematical Modeling of the Rotating Stratified Fluid in a Vicinity of the bottom of the Ocean," *International Journal of Mechanics,* vol. 13, pp. 149 - 155, 2019.

[6] I. Fetoui, "Pump Performance Curve," 28 April 2017.

[7] J. Gamboa and M. Prado, "Review of Electrical-Submersible-Pump Surging Correlation and Models," vol. 26, no. 4, 2011.

[8] Environmental, "About Submersible Pumps," WebpageFX, 2019. [Online]. Available: https://www.envisupply.com/pumps/about-submersible-pumps.htm

[9] E. Widodo and F. Ansori, "Analysis on Centrifugal Pump Performance in Single, Serial, and Parallel," *Journal of Energy, Mechanical, Material, and Manufacturing Engineering,* vol. 3, no. 2, November 2018.

[10] R. Shastri, A. K. Singh and M. K. Singh, "Analysis about losses of centrifugal pump by Matlab," *International Journal of Computational Engineering Research (IJCER),* vol. 4, no. 9, September 2014.

[11] H. Ito, "Friction Factors for Turbulent Flow in Curved Pipes," *Journal of Basic Engineering,* vol. 81, no. 2, pp. 123 - 132, 1 June 1959.

[12] K. Juckelandt, S. Bleeck and H. Wurm, "Analysis of Losses in Centrifugal Pumps with low specific speed with smooth and rough walls," in *11thEuropean Conference on Turbomachinery Fluid dynamics & Thermodynamics*, Madrid, 2015.

[13] O. C. Jones, "An Improvement in the calculation of Turbulent Friction in Recatngular Ducts," *Journal of Fluids Engineering,* June 1976.

[14] C. S. W., "Friction Factor Equation Spans all Fluid Flow Regimes," *Advances in Chemical Engineering and Science,* vol. 84, pp. 91 - 92, 1977.

[15] K. C. Thin, M. M. Khaing and K. M. Aye, "Design and Performance Analysis of Centrifugal Pump," January 2008.

[16] X. Gong and R. Chen, "Total Pressure Loss Mechanism of Centrifugal Compressors," 17 October 2014.

[17] G. Takacs, "Review of Fundamentals," in *Electrical Submerible Pumps Manual*, 2017, pp. 11 - 53.

[18] M. A. El-Naggar, "A One-Dimensional Flow Analaysis for the Prediction of Centrifugal Pump Performance Characteristics," *International Journal of Rotating Machinery,* p. 19, 29 August 2013.

[19] B. Hao, T. Lei, C. ShuLiang and L. Li, "Prediction method of impeller performance and analysis of loss mechanism for mixed-flow pump," vol. 55, 28 May 2012.

[20] E. Storteig, Dynamic characteristics and leakage performance of liquid annular seals in centrifugal pump, 1999.

[21] B. V. Esch, "Simulation of three-dimensional unsteady flow in hydraulic pumps," January 1997.

[22] J. F. Gulich, "Pumping highly visous fluids with centrifugal pump - Part 1," vol. 1999, no. 395, pp. 30 - 34, August 1999.

[23] A. Ladouani and A. Nemdili, "Influence of Reynolds number on net positive suction head of centrifugal pumps in relation to disc friction losses," vol. 73, no. 3, pp. 173-182, September 2009.

[24] G. Takacs, Electrical Submersible Pumps Manual, Elsevier Inc., 2009.

[25] J. F. Gulich, "Disk friction losses of closed turbomachine impellers," 15 March 2003.

[26] A. Pregelj, M. Drab and M. Mozetic, "Leak Detection methods and defining the sizes of leaks," in *4th International Conference of Slovenian Society for Nondestructive Testing* , Ljubljana, 1997.

[27] X. Wu, H. Liu, H. Yang, M. Tan and K. Wang, "Test and analysis on flow sepration in centrifugal pump impeller based on particle image velocimetry," *Transactions of the Chinese Society of Agricultural Engineering,* vol. 30, no. 20, 15 October 2014.

[28] M. S. Gadala and T. Halawa, "Rotating Stall simulation for axial and centrifugal compressors," *International Journal for Computational Methods in Engineering Science and Mechanics,* 1 May 2017.

[29] A. Serena, A Multiphase Pump Experimental Analysis, Skipnes Kommunikasjon, 2016.

[30] J. Andrade, M. Stanko and S. Sangesland, "Available Technologies and Performance prediction models for multiphase boosting," 7 June 2016.

[31] A. Patil, S. Gudigopuram, B. Ayyildiz, A. Delgado and G. Morrison, "Performance Evaluation and Dimensional Analysis of Multistage Helicoasxial Pump for Two-Phase Flow," *International Journal of Turbomachinery Porpulsion and Power,* 18 July 2019.

[32] J. McLoone, "Two-Phase Gas-Liquid Flow Discussion," 16 April 2019. [Online]. Available: https://fluidflowinfo.com/two-phase-gas-liquid-flow-discussion/. [Accessed 20 September 2020].

[33] E. Tahmasebi, A. Stroda, S. P. Pendli and J. Brinkerhoff, "Advances and challenges in simulation of LNG behvaiour inside a tank," in *Joint Canadian Society for Mechanical Engineering and CFD Society of Canada International Congress*, London, 2019.

[34] Y. Lim, C. J. Lee, C. Park and C. Han, "Methodology for Stable Dynamic Simulation of a LNG Pipe under Two-Phase-Flow Generation," pp. 8587-8592, 29 July 2010.

[35] W. M. Verde, J. L. Biazussi, N. A. Sassim and A. C. Bannwart, "Experimental study of gas-liquid two-phase flow patterns within centrifugal pump impellers," *Experimental Thermal and Fluid Science,* 17 Febraury 2017.

[36] M. M. Awad and Y. S. Muzychka, "Two-Phase Flow Modeling in Microchannels and Minichannels," pp. 1023 - 1033, 4 February 2011.

[37] R. Ibarra, I. Zadrazil, C. N. Markides and O. K. Matar, "Towards a Universal Dimensionless Map of flow regime transtions in Horizontal Liquid-Liquid Flows," in *11th International conference on Heat transfer, fluid mechanics and thermodynamics* , 2015.

[38] J. Zhu and H. Zhu, "A numerical study on flow patterns inside an electrical submersible pump (ESP) and comparison with visualization experiments," *Journal of Petroleum Science and Engineering,* pp. 339 - 350, 12 October 2018.

[39] J. Zhu, "CFD Simulation of ESP Performance and Bubble Size Estimation under," in *SPE Annual Technical Conference*, Amsterdam, 2014.

[40] Y. Shi, H. Zhu, B. Yin, R. Xu and J. Zhang, "Numerical Invesitgation of two-phase flow characterisitics in mutliphase pump with split vane impeller," *Journal of Mechanical Science and Technology ,* vol. 33, no. 4, 4 January 2019.

[41] H. Haario, "CFD Simulation of Two-phase and Three-phase Flows in Internal-loop Airlift Reactors," 27 May 2010.

[42] M. Murakami and K. Minemura, "Effects of Entrained Air on the Performance," *Japan Society of Mechanical Engineers,* vol. 17, no. 110, August 1974.

[43] Siew Fan Wong, Ming Chiat Law, Yudi Samyudia, Sharul Sham Dol. “Rheology Study of Water-in-Crude Oil Emulsions”. *Chemical Engineering Transactions,* vol. 45, pp. 1411-1416, 2015.

[44] S.S. Dol, M.S. Chan, S.F. Wong, J.S. Lim. "Experimental Study on the Effects of Water-in-Oil Emulsions to the Pressure Drop in Pipeline Flow". International Journal of Chemical and Molecular Engineering, vol. 10, no. 12, pp. 1528-1535, 2016.

[45] S.S. Dol, L.J. Sen. "The effect of dissipation energy on pressure drop in flow-induced oil-water emulsions pipeline", WSEAS Transactions on Environment and Development, 14, pp. 182-189, 2018.

[46] Dol, Sharul Sham, S. F. Wong, S. K. Wee, and J. S. Lim. "Experimental Study on the Effects of Water-in-oil Emulsions to Wall Shear Stress in the Pipeline Flow." Journal of Applied Fluid Mechanics vol. 11, no. 5, pp. 1309-1319, 2018.

[47] Siew Fan Wong, Sharul Sham Dol, "Turbulence Characteristics Study of the Emulsified Flow", WSEAS Transactions on heat and mass transfer, 14, pp. 45-50, 2019.

[48] Oscar Bautista, Andres Matias, Jose Arcos, Pablo Escandon, Electrokinetically- driven Viscoelastic Fluid Flow in a Microchannel with Hydrodynamic Slipwalls, Pages 1-9, Engineering World, Volume 2, 2020, ISSN: 2692-5079

Contribution of individual authors to the creation of a scientific article (ghostwriting policy)

- Salman Shahid and Abdul Qader Hasan carried out Conceptualization, writing original draft, Reviewing and editing and Formal analysis

- Omar Mustafa Kassem carried out Methodology and Writing original draft

- Dr. Sharul Sham Bin Dol, Dr. Mohamed S. Gadala and Dr. Mohamed Shiraz Aris carried out project supervision and project administration